Directly Monitoring Individual Retrovirus Budding Events Using Atomic Force Microscopy

Micha Gladnikoff and Itay Rousso
Department of Structural Biology, Weizmann Institute of Science, Rehovot 76100, Israel

ABSTRACT Retrovirus budding is a key step in the virus replication cycle. Nonetheless, very little is known about the underlying mechanism of budding, primarily due to technical limitations preventing visualization of bud formation in real time. Methods capable of monitoring budding dynamics suffer from insufficient resolution, whereas other methods, such as electron microscopy, do not have the ability to operate under physiological conditions. Here we applied atomic force microscopy to real-time visualization of individual Moloney murine leukemia virus budding events. By using a single-particle analysis approach, we were able to observe distinct patterns in budding that otherwise remain transparent. We find that bud formation follows at least two kinetically distinct pathways. The majority of virions (74%) are produced in a slow process (>45 min), and the remaining particles (26%) assemble via a fast process (<25 min). Interestingly, repetitive budding from the same site was seen to occur in only two locations. This finding challenges the hypothesis that viral budding occurs from distinct sites and suggests that budding is not restricted laterally. In this study, we established a method to monitor the fine dynamics of the virus budding process. Using this single-particle analysis to study mutated viruses will enable us to gain additional insight into the mechanisms of viral budding.

INTRODUCTION

Assembly and budding of a new virus is a fundamental step in retrovirus replication. In γ-retroviruses, such as the human immunodeficiency virus (HIV) and Moloney murine leukemia virus (MLV), both of these processes occur at the plasma membrane of the infected cell. Expression of a single viral protein, termed Gag, is sufficient to drive assembly and budding and results in the formation of virus-like particles (1,2). Gag proteins are attracted to the plasma membrane by their myristoyl group (3,4), where they associate with other Gag proteins through specific domains (5,6). Mutations of these domains were shown to significantly reduce (5,7) or even completely inhibit (8–10) virion production. Initially, self-assembly of Gag is characterized by the formation of an electron dense protein shell beneath the plasma membrane, as observed by electron microscopy (EM) (11). As the assembly process progresses, the Gag layer induces a protrusion in the plasma membrane which grows until a new virion is tethered to the cell membrane by a stalk. Lastly, the nascent virus is released from the plasma membrane by membrane fission (11). Efficient fission, in the late stages of retroviral budding, requires interactions with cellular machineries involved in the endosomal pathway (12–14). Mutations which block these interactions, either in Gag (10,15,16) or in the cellular machinery (13,17), lead to budding defects. These mutations, termed late-domain mutants, result in either arrested virions incapable of undergoing fission or the formation of multiple virus particles tethered to each other (13,18).

Retroviral budding has been extensively studied using various EM methods (19,20). Thin-section transmission EM imaging of cells infected with either HIV (11) or MLV (21) shows various stages in viral budding, starting from assembly and ending with the release of a nascent virus. Although these studies provide extensive characterization of the structural aspects of viral budding, they require sample fixation and thus lack the ability to fill a significant hole in our knowledge by providing a dynamic description of viral budding. In contrast, by using biochemical methods such as pulse chase labeling, the kinetics of viral production was studied (22). These biochemical studies provided valuable insights into the budding process, but they were limited by their ability to offer only averaged kinetics information, which made them unsuited for use in detecting the presence or otherwise of kinetically distinct budding mechanisms. Clearly, whether budding occurs through a single or multiple pathways has important implications for our understanding of its mechanism. More recently, retroviral budding from live cells has been studied by combining correlated fluorescent and scanning electron microscopy (SEM) (23). In that study, the release of single particles was followed by tracking fluorescently labeled virions. However, due to the limitations associated with optical microscopy, the formation of new virus particles could not be determined.

Despite substantial progress in the characterization of retroviral budding, the underlying physical mechanism remains poorly understood. In this study, we analyze single MLV budding events by imaging live cells with the atomic force microscope (AFM). The AFM has a similar lateral resolution to the EM, which is sufficient to image a single virus particle. Indeed, the AFM has been used to acquire high-resolution images of chemically fixed virus particles

Submitted June 9, 2007, and accepted for publication August 30, 2007.

Address reprint requests to Itay Rousso, Dept. of Structural Biology, Weizmann Institute of Science, Rehovot 76100, Israel. Tel.: 972-8-9343479; Fax: 972-8-9344136; E-mail: itay.rousso@weizmann.ac.il.

Editor: Peter Hinterdorfer.

0006-3495/08/01/320/07 $2.00

doi: 10.1529/biophysj.107.114579

(24–29) and to image nontreated virus particles and even measure their mechanical properties (30–34). In a proof of concept study, Haberle et al. demonstrated that pox virus budding can be visualized by AFM (35). We show that MLV particles bud via at least two kinetically distinct pathways. The majority of MLV particles (74%) enter an arrested state before being released, leading to a slow kinetics (>45 min). The remaining 26% bud in one continuous action and show fast kinetics (<25 min). Very rarely (<3%) were repetitive budding events observed from the same site. This observation poses a challenge to the hypothesis that viral budding occurs from unique sites on the plasma membrane. Our results are the first detailed analysis of single retrovirus budding, to our knowledge, and establish the groundwork for further detailed characterization of the viral budding mechanism.

MATERIALS AND METHODS

Cell culture

Standard NIH/3T3 murine fibroblasts and 3T3 cells stably infected with wild-type MoMLV (CL-1, a generous gift from Prof. Cunningham) were cultured as described in Fan and Paskind (36). For AFM imaging, cells were plated in 35 mm cell culture dishes and grown to ~50% confluence. Cells were typically imaged 24–48 h after plating. To maintain a high density of viral budding events, only cells which were cultured for less than 10 passages were used.

AFM imaging of live cells

AFM imaging was carried out using a Bioscope with a Nanoscope IV controller (Veeco, Santa Barbara, CA) that is mounted on an inverted optical microscope (Axiovert 200M, Carl Zeiss, Heidelberg, Germany). Images of cells were acquired in AFM tapping mode in a fluid environment. Pyramidal silicon nitride triangular cantilevers (with a nominal stiffness of 0.2 N/m (DNP)) were used. Cantilevers have a nominal tip radius of 20 nm. To properly maintain the cells, a temperature of 37°C and an atmosphere with 5% CO_2 levels were maintained during the entire duration of the measurements using a CO_2 controller (Carl Zeiss) and a temperature controller (Model 3040, Newport, Irvine, CA). This was achieved by a microincubator perfusion chamber (Model PDMI-2; Harvard Apparatus, Holliston, MA), which holds a 35 mm cell culture dish and is attached to the microscope stage.

Image rendering and kinetics analysis

Images of cells were rendered using the WSxM software (Nanotec Electronica, http://www.nanotec.es/progcorn.htm) (37). Virus particles were initially detected in the amplitude image, since it typically has better contrast than the corresponding topographic (height) image. Once virus particles were identified, their heights were determined manually by cross sectional profiles from the topographic images. In this method, single particles were tracked frame by frame to extract their budding kinetics pattern.

Electron microscopy

Cells were cultured on a microscope cover glass and fixed by incubation with a solution of 2% glutaraldehyde (EM grade) in 0.1 M sodium cacodylate, pH 7.3 for at least 50 min at room temperature. After fixation, samples were immersed in 0.1% tannic acid for 20 min and rinsed in distilled water, followed by 20 min incubation in 0.1% uranyl acetate solution. After rinsing, samples were dehydrated by a series of solutions having increasing ethanol concentrations, followed by critical point drying with liquid CO_2. Samples were sputter coated with a layer of 10 nm chromium. Cells and viruses were viewed and photographed using an environmental scanning electron microscope (Phillips XL-30, FEI, Eindhoven, The Netherlands).

RESULTS

Imaging MLV budding from live cells

Budding of MLV particles was imaged with the AFM operated in tapping mode to minimize possible damage to cells by the AFM probe (Fig. 1, *A* and *B*). For this study, the cell line used was CL-1, which originates from a standard NIH/3T3 mouse fibroblast cell line that is chronically infected with MLV (36). To maintain the health of the cells throughout the entire duration of the measurements, both the temperature and CO_2 levels were controlled. Viability of the

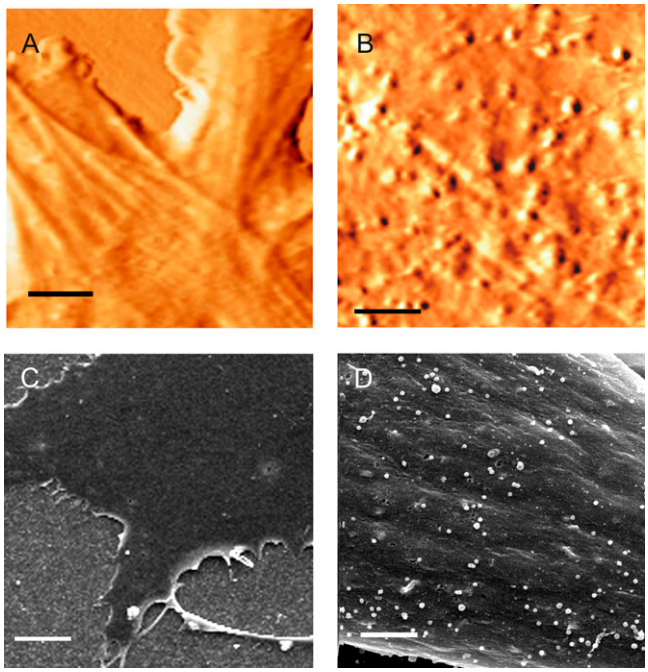

FIGURE 1 AFM and SEM images of uninfected and MLV infected cells. (*A*) An AFM amplitude image, acquired in tapping mode, of an uninfected NIH/3T3 live cell. The apparent fibril structures underneath the cell membrane are likely to be associated with the cytoskeleton. Scan area is 24 × 24 μm, 410 × 410 pixels. Scale bar is 5 μm. (*B*) A tapping mode AFM image of an MLV infected NIH/3T3 live cell (CL-1). Virus particles at different stages of budding appear as protrusions of different heights on the cell membrane. Due to convolution between the AFM tip and the virus, these protrusions appear larger than their actual dimensions. Scan area is 15 × 15 μm, 512 × 512 pixels. Scale bar is 3 μm. SEM images of an uninfected NIH/3T3 cell (*C*) and of a CL-1 cell (*D*). Budding virus particles are clearly observed at the CL-1 cell surface. The density of budding events is similar to what is seen in the AFM images. Virions have native-like dimensions with diameter of ~120 nm. Scale bar in *C* and *D*, is 1 and 2 μm, respectively.

cells was constantly inspected using standard optical microscopy. With this setup, cells remained viable and healthy for durations exceeding 5 h.

Images of a noninfected NIH/3T3 cell show a relatively smooth membrane surface (Fig. 1 *A*). Often it is possible to identify in the AFM images, fibril structures beneath the cellular membrane, and these are likely to be cellular cytoskeletal elements. In contrast to noninfected cells, images of the surface of MLV infected CL-1 cells reveal a large amount of virus particles at different stages of budding. This is indicated by apparent protrusions of different heights from the cellular membrane (Fig. 1 *B*). The width of the particles appears to be larger than their native dimensions (80–150 nm) (38) due to convolution between the AFM tip and the virus. Therefore, for the purpose of determining virus dimensions, their width is less accurate than their height. As a control, noninfected NIH/3T3 and CL-1 cells were imaged by SEM (Fig. 1, *C* and *D*). Similarly to our AFM images, SEM imaging of noninfected cells shows a smooth membrane surface, whereas imaging of CL-1 membrane shows its surface to be covered with virus particles having a native width of ~120 nm in diameter (i.e., within the range of their actual dimensions). Usually we find that viral density decreases with increasing cell passage numbers. We therefore imaged cells that had been passaged up to a maximum of 10 times.

Typically, an extremely high concentration of particles on the cell surface was found during the initial two scans. Thereafter, the concentration of particles dropped, and budding sites were more easily detected.

Real-time imaging of MLV budding

To image budding events with the potential to follow several budding cycles, cells were imaged repetitively for durations ranging 1–3 h. Scan areas were set at 10 × 10 μm to maximize the number of captured budding events. Frequently, scanning areas were decreased to zoom in on specific virus particles. Depending on the scan size, imaging of a single frame took 2–7 min. The resolution of the AFM is particularly high (subnanometer) in the *z*-direction (height), which makes it a powerful tool for monitoring viral budding.

The progress of viral budding was determined by measuring the viral protrusion height as a function of time. Viral heights were determined manually from their cross sectional profiles (Fig. 2). In this method, single particles were tracked frame by frame to extract their budding kinetics pattern. Overall, 64 trajectories of budding events were analyzed in this study (Fig. 3 *A*). The majority of events (47 events, 74%) incorporated a phase during which viral growth was arrested. This phase began when the virus reached a height near or equal to its maximal height (Fig. 3, *B–D*). These budding trajectories were slow and lasted for over 45 min. Out of these slow events, we were able to monitor only two complete trajectories, which were composed of three distinct phases: viral growth, an arrested phase, and a viral release phase (Fig. 3 *B*). In all other cases, only minimal lifetime values could be estimated because partial trajectories were captured that covered only the first two (growth and stalled; Fig. 3 *C*) or last two (stalled and release) phases (Fig. 3 *D*), or just the arrested phase alone (not shown).

The remaining 17 events (26%) exhibited no arrested phase, which gave rise to faster budding kinetics (Fig. 3 *A*, *gray column*, and *E–G*). All of the fast kinetics trajectories covered both the growth phase and the release of the newly formed virus and were completed in less than 25 min. Interestingly, all fast events had similar growth kinetics of ~10 min. By contrast, the release phase varies between 10 and 15 min and appears to be cell specific. The averaged trajectories of budding from three cells are shown in Fig. 3, *E–G*.

When viewing earlier segments of the budding trajectory, specifically, the frames immediately before a particle was detected, we occasionally observed an elevated region with an area larger than that of a virus (1–2 μm in diameter). In addition, often after release of virions, features with heights slightly larger (~15–20 nm) than the topography of the cell membrane surroundings remained visible at the site from which the newly released virion had budded (Fig. 3, *E–G*, *arrows*). These features were no longer detectable during the following scan, which occurred after roughly 5 min. Further imaging of this area did not show a regrowth of its height.

Out of all visualized budding sites, successive release of virus particles from the same location was observed at only two sites. At one site, four budding events were detected,

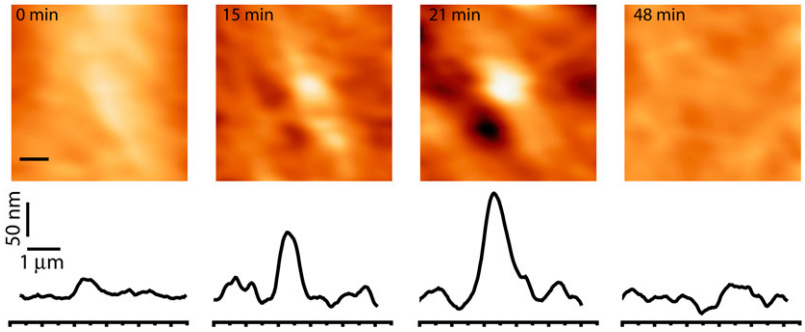

FIGURE 2 Visualizing a complete budding progress, from initial assembly to release of a single virus particle. AFM height topographic time series images of a virus particle emerging from live cells (*upper panel*), with their corresponding cross sectional profiles (*lower panel*). At t = 0 min, the emerging bud is seen as a minor protrusion, located in the center of a larger area that is slightly elevated from the surrounding cell membrane. After ~20 min, the bud virion has grown to its maximal height and is released after an additional 28 min (t = 48 min). Image scan area is 3.1 × 3.1 μm, 80 × 80 pixels. Scale bar is 0.5 μm.

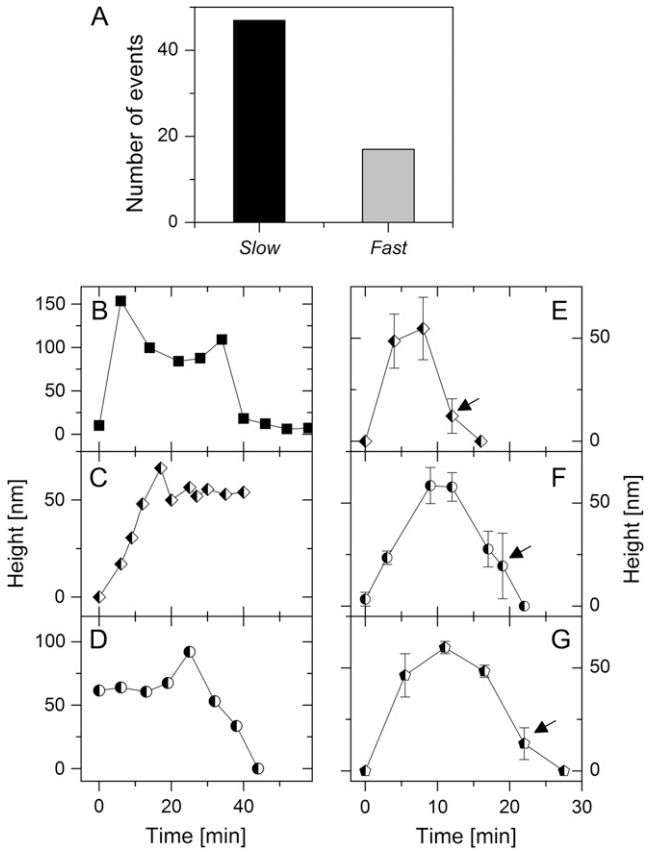

FIGURE 3 Analysis of the kinetics of single MLV budding events. (*A*) All analyzed budding events (64 in total) can be divided into two main groups according to their kinetics profiles: 17 (26%) of the budding events take place without an arrested phase, giving rise to fast budding kinetics lasting less than 25 min (*gray*). The remaining 47 (74%) events are characterized by a slow budding kinetics, having a lifetime longer than 45 min (*black*). Out of these slow budding events, two events (4%) were captured that contain a complete kinetics trajectory, including the growth, arrested, and release phases (*B*). The remaining slow budding trajectories were partially captured, with images obtained of either their first two (growth and arrested; *C*) or last two (arrested and release, *D*) phases. (*E–G*) Averaged trajectories of fast budding events measured from three different cells ($n = 4$, 3, and 4, respectively). In contrast to the growth rate, which is very similar for all three cells, slight differences are observed in the release rate (see portion of *curve* indicated by an *arrow*). Features of 15–20 nm in height are detected ~5 min before the budding site attains its initial height.

whereas only two successive events were detected from the second site (Fig. 4) during the duration of the measurement. Intriguingly, all the consecutive budding event trajectories were nearly identical and fast (~12 min for each event). Moreover, the events occurred continuously without any observable lag between single events.

Often, particles appeared to be moving slowly in a specific direction on the cell surface (Fig. 5). The directions of movement of different buds were normally independent of each other. Budding particles were frequently, but not always, found in proximity to a cytoskeleton element and in some cases appeared to travel along cellular stress fibers.

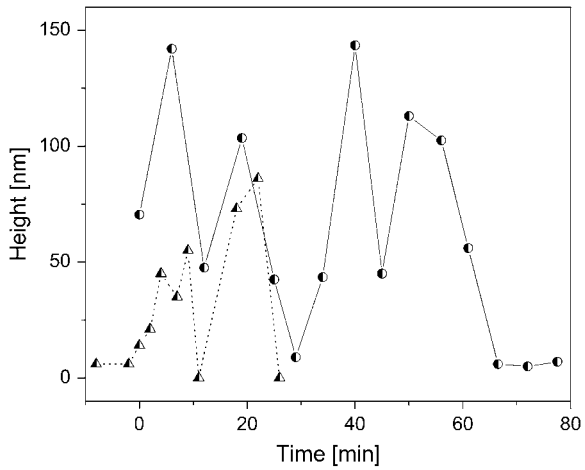

FIGURE 4 Consecutive budding events from the same site. Graph shows height changes as a function of time measured at two locations. At one site, four rapid repetitive events are detected (*solid line*), whereas two events are detected at the second site (*dashed line*). Within the limitation of our experimental temporal resolution, no lag time between events is detected.

DISCUSSION

In this study, real time budding of MLV particles was monitored and analyzed using AFM. Live cells were continuously imaged for several hours, during which multiple budding events from the cells' apical surface were recorded. The AFM is capable of tracing budding of a single virus due to its high topographical resolution. To the best of our knowledge, this is the first detailed analysis of single retrovirus particle budding events. In contrast to bulk measurements of viral budding, single particle analysis can identify patterns in budding, as well as different pathways characterized by distinct kinetics. Indeed, we have found that MLV budding occurs through at least two pathways, one characterized by fast kinetics, and the other by slow kinetics. Whereas the fast pathway was characterized by growth of the newly formed particle to its maximal height followed by rapid release, the slow pathway included a stationary or arrested phase between the growth and release phases, in which the height of the particle remained unchanged. Intuitively, one would speculate that particles in this arrested phase represent virions which have completed their budding process but are trapped on the plasma membrane. If this were the case, these trapped virus particles would likely be released from the plasma membrane during image acquisition by the sheer force of the scanning AFM probe, similarly to the manner in which the initial high density of virus particles typically observed on the cell's plasma membrane during the first scan was mostly gone by the following image. Yet this did not occur, with the newly formed virion bud remaining visible over subsequent scans. We therefore conclude that the arrested phase is an integral part of the slow budding pathway.

The mechanism underlying the observed slow and fast budding pathways cannot be conclusively determined at this

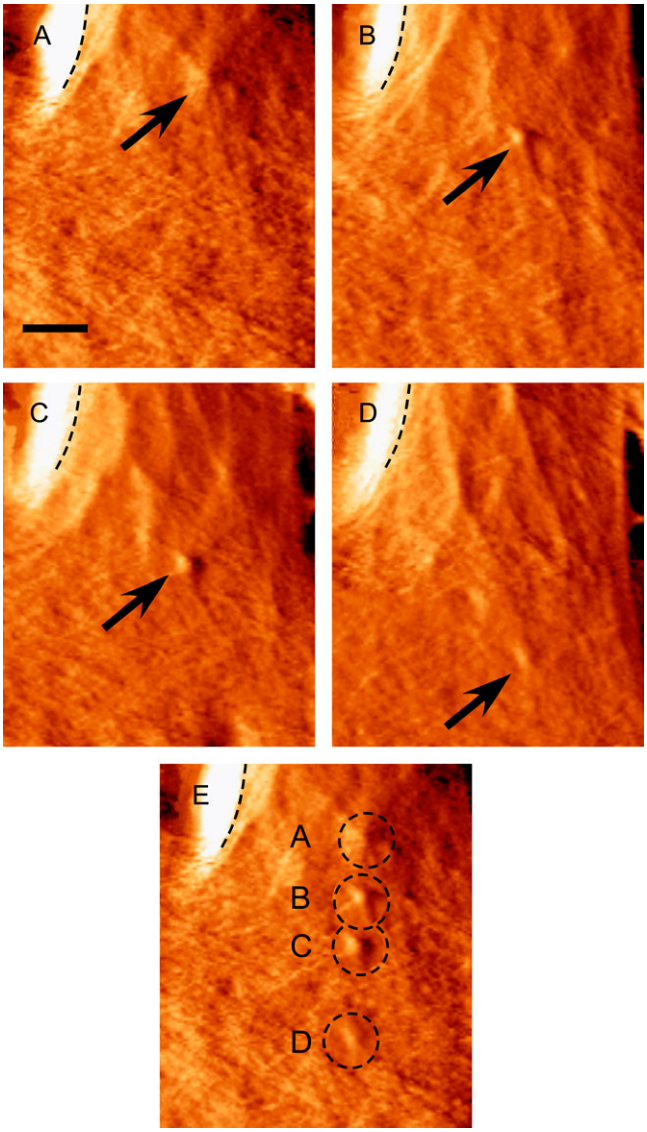

FIGURE 5 The movement of a virus on the cell surface. AFM height topographic time series images of a virus particle (*A–D*). Images were acquired at intervals of 6 min. Aligning images using as a reference point the cell border (*black dashed line*) and overlaying them on top of each other (*E*), reveals a clear directional movement. Scale bar is 2 μm.

stage. However, it may be related to several possible processes. In general, viral budding can be divided into two main steps: the assembly of viral proteins at the cell membrane, which causes it to bend, and the pinching off of the nascent virus from the membrane. In all of our measurements, the arrested phase appeared after the virion had attained its full, or nearly full, size. Furthermore, the growth rate of virion particles was found to be very similar for all analyzed particles, regardless of their overall kinetics. It is therefore reasonable to assume that the arrested state is associated with the fission step rather than with the assembly step. Recent experimental evidence suggests that efficient fission requires recruitment of cellular factors involved in the endosomal pathways (14). Poor incorporation of these cellular machinery factors may give rise to the observed stalled phase of the slow budding events. An additional protein that could impact budding kinetics is viral protease (PR). PR has been suggested to play a role in the budding process, though the mechanism is mostly unknown (15,16,39). Alternatively, the observed two budding kinetics may represent different Gag protein assembly pathways. Although we cannot completely rule out this possibility, we consider it unlikely, since different packaging of Gag will result in different virus growth rates. Future studies of genetically modified virus particles may provide more insights into the mechanisms which give rise to the kinetically different budding pathways as, for example, inactivated PR or late-domain mutations are known to affect virus release.

Comparison between fast budding events originating from different cells reveals differences primarily in their release rate, rather than in their growth rate (Fig. 3, *E–G*). Interestingly, we find that the fast budding trajectories of particles released from the same cell are nearly identical. Several biophysical models suggest that the fission step represents an energetic barrier (40). These models are supported by experimental evidence which suggests that ATP is required for fission (41). It is therefore possible that differences in the biochemical activities between cells give rise to the observed variations in viral release.

One of the open questions in retroviral budding is associated with budding sites. Specifically, are there unique sites on the plasma membrane for viral budding? Probably the strongest evidence supporting an affirmative answer to this question comes from studies in which mutations were introduced to the late domain of Gag (10,13). In these studies, chains of virions have been observed extending from the plasma membrane, suggesting that virus budding occurs from a distinct site on cell surfaces. Several other studies suggest that lipid rafts act as platforms for virus assembly and budding (reviewed in Briggs et al. (42)). Our results suggest that viral budding does not occur from unique sites. Repetitive formation of virus particles from the same site was observed in only two sites (~3%). This finding does not contradict the hypothesis according to which viral budding occurs from lipid rafts, since rafts are thought to exist as a rather dynamic and fluid state (43). However, our findings contradict the conclusion, drawn from late-domain HIV-1 mutants, that there exist unique sites for viral budding on the cell membrane. This discrepancy can be explained by differences in the budding of wild-type versus late-domain mutant viruses.

Preassembly and postbudding structural features

A striking and frequent observation was of structural features that appeared during the preassembly stage and/or after the nascent virus had been released. We consider the preassembly

state as being the time point preceding the first image in which a membrane protrusion is identified. The observed structural feature in this early state is characterized by a slightly elevated region whose area (diameter of 1–2 μm) is significantly larger than that of a virus. This structural feature may represent an initial assembly of Gag proteins underneath the plasma membrane. Alternatively, this feature may be an indication of a rearrangement of the cell cytoskeleton.

A similar elevated structural feature was also observed after the virus had been released from the cell membrane. However, in contrast to the larger preassembly feature, this structure has an area similar to that of a virus particle. Typically, 10–20 min after the release of the virion, this slightly elevated structure (15–20 nm) disappears. In this case, we speculate that the observed structure is unlikely to represent Gag subunits. If it were composed of Gag proteins, we would expect that a consecutive budding event would take place from this site instead of it being dissolved. Our results suggest that this is not the case, since repetitive budding events from a single site were observed in only two locations (3%). We therefore conclude that the observed structure may contain cytoskeletal elements, or alternatively it may represent budding machinery, such as the ESCRT (endosomal sorting complex required for transport) complexes (14), which has yet to disassemble.

In conclusion, we have shown that single virus budding events can be visualized using AFM. By using a single-particle analysis approach, distinct patterns normally transparent in bulk measurements were observed. We discovered that viral budding follows two kinetically distinct pathways. The results of this study have implications for our understanding of the mechanisms underlying virus assembly and budding. Future studies combining a single-particle approach with mutated virions hold great potential to provide new insights into the mechanism that governs viral assembly and budding.

The wild-type MoMLV (CL-1) from which we cultured the cells used in these experiments was a generous gift from Prof. Cunningham. We thank Orna Yeger for her help with sample preparation for SEM analysis, and Heli Gueta for her assistance in SEM image acquisition.

This work was supported in part by a grant from the Clore Center for Biological Physics, Jean-Jacques Brunschwig Fund for the Molecular Genetics of Cancer, and the Kimmelman Center for Macromolecular Assemblies. I.R. is the incumbent of the Robert Edwards and Roselyn Rich Manson Career Development Chair.

REFERENCES

1. Gheysen, D., E. Jacobs, F. de Foresta, C. Thiriart, M. Francotte, D. Thines, and M. De Wilde. 1989. Assembly and release of HIV-1 precursor Pr55gag virus-like particles from recombinant baculovirus-infected insect cells. *Cell.* 59:103–112.
2. Wills, J. W., and R. C. Craven. 1991. Form, function, and use of retroviral Gag proteins. *AIDS.* 5:639–654.
3. Gottlinger, H. G., J. G. Sodroski, and W. A. Haseltine. 1989. Role of capsid precursor processing and myristoylation in morphogenesis and infectivity of human immunodeficiency virus type 1. *Proc. Natl. Acad. Sci. USA.* 86:5781–5785.
4. Rein, A., M. R. McClure, N. R. Rice, R. B. Luftig, and A. M. Schultz. 1986. Myristylation site in Pr65gag is essential for virus particle formation by Moloney murine leukemia virus. *Proc. Natl. Acad. Sci. USA.* 83:7246–7250.
5. Cheslock, S. R., D. T. Poon, W. Fu, T. D. Rhodes, L. E. Henderson, K. Nagashima, C. F. McGrath, and W. S. Hu. 2003. Charged assembly helix motif in murine leukemia virus capsid: an important region for virus assembly and particle size determination. *J. Virol.* 77:7058–7066.
6. Mammano, F., A. Ohagen, S. Hoglund, and H. G. Gottlinger. 1994. Role of the major homology region of human immunodeficiency virus type 1 in virion morphogenesis. *J. Virol.* 68:4927–4936.
7. Zhou, W., L. J. Parent, J. W. Wills, and M. D. Resh. 1994. Identification of a membrane-binding domain within the amino-terminal region of human immunodeficiency virus type 1 Gag protein which interacts with acidic phospholipids. *J. Virol.* 68:2556–2569.
8. Auerbach, M. R., K. R. Brown, A. Kaplan, D. de Las Nueces, and I. R. Singh. 2006. A small loop in the capsid protein of Moloney murine leukemia virus controls assembly of spherical cores. *J. Virol.* 80:2884–2893.
9. Auerbach, M. R., C. Shu, A. Kaplan, and I. R. Singh. 2003. Functional characterization of a portion of the Moloney murine leukemia virus Gag gene by genetic footprinting. *Proc. Natl. Acad. Sci. USA.* 100: 11678–11683.
10. Gottlinger, H. G., T. Dorfman, J. G. Sodroski, and W. A. Haseltine. 1991. Effect of mutations affecting the p6 Gag protein on human immunodeficiency virus particle release. *Proc. Natl. Acad. Sci. USA.* 88:3195–3199.
11. Gelderblom, H. R., E. H. Hausmann, M. Ozel, G. Pauli, and M. A. Koch. 1987. Fine structure of human immunodeficiency virus (HIV) and immunolocalization of structural proteins. *Virology.* 156:171–176.
12. Freed, E. O. 2002. Viral late domains. *J. Virol.* 76:4679–4687.
13. Garrus, J. E., U. K. von Schwedler, O. W. Pornillos, S. G. Morham, K. H. Zavitz, H. E. Wang, D. A. Wettstein, K. M. Stray, M. Cote, R. L. Rich, D. G. Myszka, and W. I. Sundquist. 2001. Tsg101 and the vacuolar protein sorting pathway are essential for HIV-1 budding. *Cell.* 107:55–65.
14. Morita, E., and W. I. Sundquist. 2004. Retrovirus budding. *Annu. Rev. Cell Dev. Biol.* 20:395–425.
15. Huang, M., J. M. Orenstein, M. A. Martin, and E. O. Freed. 1995. p6Gag is required for particle production from full-length human immunodeficiency virus type 1 molecular clones expressing protease. *J. Virol.* 69:6810–6818.
16. Yuan, B., X. Li, and S. P. Goff. 1999. Mutations altering the Moloney murine leukemia virus p12 Gag protein affect virion production and early events of the virus life cycle. *EMBO J.* 18:4700–4710.
17. Segura-Morales, C., C. Pescia, C. Chatellard-Causse, R. Sadoul, E. Bertrand, and E. Basyuk. 2005. Tsg101 and Alix interact with murine leukemia virus Gag and cooperate with Nedd4 ubiquitin ligases during budding. *J. Biol. Chem.* 280:27004–27012.
18. Yuan, B., S. Campbell, E. Bacharach, A. Rein, and S. P. Goff. 2000. Infectivity of Moloney murine leukemia virus defective in late assembly events is restored by late assembly domains of other retroviruses. *J. Virol.* 74:7250–7260.
19. Demsey, A., and R. M. Friedman. 1983. Reexamination of the morphogenetic block of a putative late-stage, temperature-sensitive mutant of Moloney murine leukemia virus. *J. Virol.* 45:1140–1142.
20. Gonda, M. A., R. V. Gilden, and K. C. Hsu. 1979. An unlabeled antibody macromolecule technique using hemocyanin for the identification of type B and type C retrovirus envelope and cell surface antigens by correlative fluorescence, transmission electron, and scanning electron microscopy. *J. Histochem. Cytochem.* 27:1445–1454.
21. Yuen, P. H., and P. K. Wong. 1977. Electron microscopic characterization of the defectiveness of a temperature-sensitive mutant of Moloney murine leukemia virus restricted in assembly. *J. Virol.* 24:222–230.
22. Tritel, M., and M. D. Resh. 2000. Kinetic analysis of human immunodeficiency virus type 1 assembly reveals the presence of sequential intermediates. *J. Virol.* 74:5845–5855.

23. Larson, D. R., M. C. Johnson, W. W. Webb, and V. M. Vogt. 2005. Visualization of retrovirus budding with correlated light and electron microscopy. *Proc. Natl. Acad. Sci. USA.* 102:15453–15458.

24. Kuznetsov, Y. G., S. Datta, N. H. Kothari, A. Greenwood, H. Fan, and A. McPherson. 2002. Atomic force microscopy investigation of fibroblasts infected with wild-type and mutant murine leukemia virus (MuLV). *Biophys. J.* 83:3665–3674.

25. Kuznetsov, Y. G., J. G. Victoria, W. E. Robinson Jr., and A. McPherson. 2003. Atomic force microscopy investigation of human immunodeficiency virus (HIV) and HIV-infected lymphocytes. *J. Virol.* 77:11896–11909.

26. Kuznetsov, Y. G., A. Low, H. Fan, and A. McPherson. 2004. Atomic force microscopy investigation of wild-type Moloney murine leukemia virus particles and virus particles lacking the envelope protein. *Virology.* 323:189–196.

27. Kuznetsov, Y. G., J. G. Victoria, A. Low, W. E. Robinson Jr., H. Fan, and A. McPherson. 2004. Atomic force microscopy imaging of retroviruses: human immunodeficiency virus and murine leukemia virus. *Scanning.* 26:209–216.

28. Kuznetsov, Y. G., A. Low, H. Fan, and A. McPherson. 2005. Atomic force microscopy investigation of isolated virions of murine leukemia virus. *J. Virol.* 79:1970–1974.

29. Kuznetsov, Y. G., and A. McPherson. 2006. Identification of DNA and RNA from retroviruses using ribonuclease A. *Scanning.* 28: 278–281.

30. Carrasco, C., A. Carreira, I. A. Schaap, P. A. Serena, J. Gomez-Herrero, M. G. Mateu, and P. J. de Pablo. 2006. DNA-mediated anisotropic mechanical reinforcement of a virus. *Proc. Natl. Acad. Sci. USA.* 103:13706–13711.

31. Ivanovska, I. L., P. J. de Pablo, B. Ibarra, G. Sgalari, F. C. MacKintosh, J. L. Carrascosa, C. F. Schmidt, and G. J. Wuite. 2004. Bacteriophage capsids: tough nanoshells with complex elastic properties. *Proc. Natl. Acad. Sci. USA.* 101:7600–7605.

32. Kol, N., M. Gladnikoff, D. Barlam, R. Z. Shneck, A. Rein, and I. Rousso. 2006. Mechanical properties of murine leukemia virus particles: effect of maturation. *Biophys. J.* 91:767–774.

33. Kol, N., Y. Shi, M. Tsvitov, D. Barlam, R. Z. Shneck, M. S. Kay, and I. Rousso. 2007. A stiffness switch in human immunodeficiency virus. *Biophys. J.* 92:1777–1783.

34. Michel, J. P., I. L. Ivanovska, M. M. Gibbons, W. S. Klug, C. M. Knobler, G. J. Wuite, and C. F. Schmidt. 2006. Nanoindentation studies of full and empty viral capsids and the effects of capsid protein mutations on elasticity and strength. *Proc. Natl. Acad. Sci. USA.* 103: 6184–6189.

35. Haberle, W., J. K. H. Horber, F. Ohnesorge, D. P. E. Smith, and G. Binnig. 1992. In situ investigations of single living cells infected by viruses. *Ultramicroscopy.* 42:1161–1167.

36. Fan, H., and M. Paskind. 1974. Measurement of the sequence complexity of cloned Moloney murine leukemia virus 60 to 70S RNA: evidence for a haploid genome. *J. Virol.* 14:421–429.

37. Horcas, I., R. Fernandez, J. M. Gomez-Rodriguez, J. Colchero, J. Gomez-Herrero, and A. M. Baro. 2007. WSXM: a software for scanning probe microscopy and a tool for nanotechnology. *Rev. Sci. Instrum.* 78:013705.

38. Yeager, M., E. M. Wilson-Kubalek, S. G. Weiner, P. O. Brown, and A. Rein. 1998. Supramolecular organization of immature and mature murine leukemia virus revealed by electron cryo-microscopy: implications for retroviral assembly mechanisms. *Proc. Natl. Acad. Sci. USA.* 95:7299–7304.

39. Bowles, N., D. Bonnet, F. Mulhauser, and P. F. Spahr. 1994. Site-directed mutagenesis of the P2 region of the Rous sarcoma virus Gag gene: effects on Gag polyprotein processing. *Virology.* 203:20–28.

40. Chernomordik, L. V., and M. M. Kozlov. 2003. Protein-lipid interplay in fusion and fission of biological membranes. *Annu. Rev. Biochem.* 72:175–207.

41. Tritel, M., and M. D. Resh. 2001. The late stage of human immunodeficiency virus type 1 assembly is an energy-dependent process. *J. Virol.* 75:5473–5481.

42. Briggs, J. A., T. Wilk, and S. D. Fuller. 2003. Do lipid rafts mediate virus assembly and pseudotyping? *J. Gen. Virol.* 84:757–768.

43. Simons, K., and E. Ikonen. 1997. Functional rafts in cell membranes. *Nature.* 387:569–572.